Hierarchical Modeling O_2 and N_2 Adsorption in C_{168} Schwarzite: From Quantum Mechanics to Molecular Simulation

Jianwen Jiang,* Jeffery B. Klauda, and Stanley I. Sandler

Center for Molecular and Engineering Thermodynamics, Department of Chemical Engineering, University of Delaware, Newark, Delaware, 19716

Received: December 17, 2003; In Final Form: March 23, 2004

The adsorption of pure O_2 and N_2 and their mixture in C_{168} schwarzite, as a model for a nanoporous carbon adsorbent, has been studied with use of grand canonical Monte Carlo simulations. The gas−carbon interaction is modeled by a pairwise additive atom−atom Lennard-Jones potential with parameters determined from ab initio quantum mechanical computations. For pure O_2, the adsorption simulated with the ab initio potential is similar to that with the empirical Steele potential derived from gas adsorption on planar graphite in the limit of zero loading; however, for pure N_2, the adsorption simulated with the ab initio potential is much larger. Consequently, a large adsorption selectivity of N_2 over O_2 from their mixture is found with the ab initio potential. With both potentials the adsorbed gas molecules are found to preferentially align along the channel intersection of the C_{168} schwarzite structure, and a localized nonuniform density distribution of the adsorbed gas molecules is observed, which is more evident with the ab initio potential. The predictions of mixture adsorption using the ideal-adsorbed-solution theory based on the adsorption of only the pure gases agree well with the simulations. This work demonstrates the importance of an accurate adsorbate−adsorbent interaction potential in the determination of gas adsorption behavior, and suggests that nanoporous carbon membranes might be useful for air separation.

I. Introduction

Recent experiments by Foley and co-workers[1,2] show that the nanoporous carbon (NPC) membranes synthesized by ultrasonic deposition may be useful for the separation of gases with similar molecular dimensions. For example, at room temperature, the permeance of O_2 was found to be from 2 to 30 times larger than that of N_2 depending on the NPC synthesis conditions. These NPC membranes may lead to more efficient gas separation processes. To elucidate the underlying physics behind this unusually high separation, we have investigated the adsorption of pure O_2 and N_2 and their mixture in an NPC using a graphite-based adsorbate−adsorbent potential.[3,4] Since the amorphous NPC membranes synthesized by Foley et al.[1,2] do not have well-defined structures, as a model, the hypothetical C_{168} schwarzite was used due to its simple periodic structure with well-defined pores and channels. Although the structures of an NPC and the C_{168} schwarzite differ, the carbon surface curvatures are similar, so that segments of the C_{168} schwarzite may provide a similar environment for adsorbates as found experimentally in an NPC. In these studies,[3,4] the gas−carbon interaction was modeled by the pairwise additive atom−atom Lennard-Jones potential and the commonly used potential parameters derived by Steele and co-workers[5,6] from the adsorption of gases on planar graphite in the limit of zero loading. Using this empirical Steele potential, we found that the extent of the adsorption of pure O_2 and N_2 in the C_{168} schwarzite is very similar, so that the adsorption selectivity of O_2 to N_2 from a binary mixture is small.

The prevailing explanation for the large difference in permeability between O_2 and N_2 is the slightly smaller size of O_2, which would be solely an entropic effect. That is, the activation entropy of transport would be lower for O_2 than N_2. However, molecular-level studies[7,8] with transition-state theory have demonstrated that the entropic argument does not dominate, instead, an enthalpic effect might be responsible for the large separation between O_2 and N_2, in which case, the gas−carbon interaction potential is the determinant factor. The use of the empirical Steele potential from gas adsorption on planar graphite for the interaction between a gas and the C_{168} schwarzite is an approximation based on the assumption that the C_{168} schwarzite can be treated as wrapped graphene sheets. However, the gas−carbon interaction potential might be influenced by the curvature and the ring structure of the carbon atoms. A curved carbon surface increases the localization of the electron density, causing a shift in the hybridization of the carbon atoms and the ring structures. Consequently, an improvement of the interaction potential accounting for the effects of curvature and ring structure is needed to more accurately describe gas adsorption, as an inaccurate potential will lead to large errors.[9]

Quantum mechanical computations are playing increasingly important roles in chemical and physical sciences, and in chemical engineering.[10] Using such first-principles computations one can obtain accurate interaction potentials and then through simulation determine the macroscopic properties. In this work we have used a hierarchical approach to model gas adsorption in the C_{168} schwarzite. First, we obtain accurate ab initio gas−carbon interaction potentials from quantum mechanics, and then compute adsorption behavior from atomistic molecular simulation. As we shall see, with the ab initio potential, we find a large difference in the adsorption between O_2 and N_2 in the C_{168} schwarzite, which is not the case when using the Steele potential.

In Section II we describe briefly the models used for the adsorbent and adsorbate, and the quantum mechanical ab initio

* Corresponding author. E-mail: jiangj@che.udel.edu. Phone: 302-831-6953. Fax: 302-831-1048.

10.1021/jp0379087 CCC: $27.50 © 2004 American Chemical Society
Published on Web 05/18/2004

TABLE 1: Atom−Atom Lennard-Jones Potential Parameters

			Steele potential		ab initio potential	
	O−O	N−N	C−O	C−N	C−O	C−N
σ (Å)	2.99	3.32	3.19	3.36	3.269	3.542
ϵ/k_B (K)	52.0	36.4	37.6	33.4	35.128	36.902
l (Å)	1.208	1.10				

potential obtained in this study, followed in Section III by the methods used, including the Monte Carlo method to simulate the adsorption of both pure and mixed gases, and the ideal-adsorbed-solution theory to predict the mixture adsorption. The results for the adsorption isotherm, adsorption energy, heat of adsorption, center-of-mass density distribution, and molecular orientation within the adsorbent calculated with both the ab initio potential and the empirical Steele potential are presented and compared in Section IV. Finally conclusions are given in Section V.

II. Model and Potential

As in previous studies,[3,4] C_{168} schwarzite[11] is used to represent the adsorbent NPC membrane. In addition to six-membered rings in planar graphite, there are seven-membered rings in the C_{168} schwarzite with a unit cell length of 21.8 Å, and 672 carbon atoms. There are two types of pores in the C_{168} schwarzite with average diameters of about 7 and 9 Å. The pores in the same layer are isolated from each other, but they are connected with those in the neighboring layers by channel intersections at about 45° (and 135° by symmetry) from the z axis. The carbon−carbon bonds are assumed to be rigid, and the locations of the carbon atoms are frozen during the simulation. These assumptions should not notably affect adsorption, but may influence the transport properties (which are not considered here). The adsorbates, O_2 and N_2, are represented as rigid diatomic molecules interacting with an isotropic atom−atom Lennard-Jones potential. The potential parameters[12,13] are given in Table 1, and the Lorentz−Berthelot combining rules are used to calculate the cross interactions in the O_2 and N_2 mixture.

The gas−carbon interaction is modeled by using the pairwise additive atom−atom Lennard-Jones potential. The potential parameters used in the previous studies[3,4] were derived from gas adsorption on planar graphite.[5,6] To account for the curvature and the ring structure of the carbon surface, in this work the potential parameters are obtained from the quantum mechanical Hybrid Method for Interaction Energies (HM-IE), which we have recently developed.[14,15] The method can be used to accurately approximate the interaction energies from a high-level method with a large basis set while requiring considerably less computational time and resources, and has been tested for a variety of systems, including for the interaction energies of Ne_2, $(C_2H_2)_2$, and N_2-benzene. To compute the interaction energies for the large system in this study, the C_{168} schwarzite was cut into smaller pieces to accelerate the calculations. For details, see ref 15, in which the interaction energies of O_2 and N_2 with C_{168} schwarzite and C_{60} buckyball, respectively, have been obtained with this method. All computations were performed with the Gaussian 98 suite of programs,[16] and the calculated ab initio interaction energies were fitted to the pairwise atom−atom Lennard-Jones potential resulting in the parameters given in Table 1. To clarify, by using the HM-IE method to calculate the interaction energies between an adsorbate molecule with the C_{168} schwarzite, all contributions including electrostatic interactions are taken into account from first principles. For ease in molecular simulation, however, the interaction energies were then fitted to a Lennard-Jones potential, though a more sophisticated potential might have been used to fit. This is also the case for the Steele potential,[5,6] where the Lennard-Jones potential was used to fit experimental adsorption properties on planar graphite.

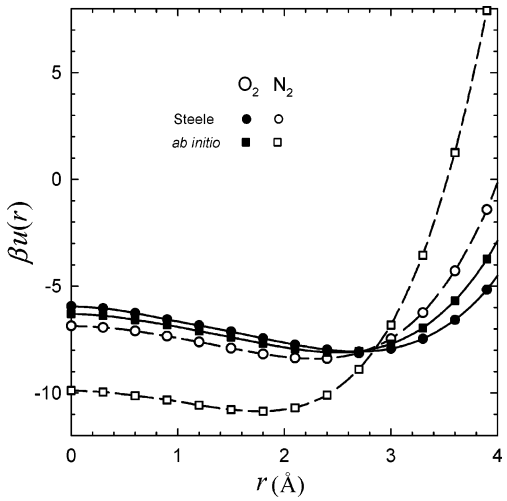

Figure 1. Interaction energies of O_2 and N_2 molecules, respectively, with the channel intersection of the C_{168} schwarzite, where r is the distance from the center of the channel intersection. The solid (O_2) and open (N_2) circles are the Steele potential, the solid (O_2) and open (N_2) squares are the ab initio potential, and the lines are to guide the eye.

In ref 15 we have shown that our HM-IE based potential for graphite can accurately predict experimental 2nd virial coefficients of adsorption for N_2 on graphite sheets. The curvature and the ring structure in the C_{168} schwarzite are different from those of planar graphite, leading to the differences between the parameter values of the ab initio potential developed here and the Steele potential. The values of the collision diameter σ vary the most between the two potentials, though there is also a small difference in the values of the well depth ϵ. The values of σ_{C-N} and σ_{C-O} in the ab initio potential are larger, and ϵ_{C-N} is larger and ϵ_{C-O} is smaller than in the Steele potential. These differences in the two potentials can result in large energy differences for gases interacting with the C_{168} schwarzite.

Figure 1 shows the interaction energies of an O_2 and N_2 molecule, respectively, in the tetrahedral channel intersection of the C_{168} schwarzite, which contains 120 carbon atoms within a 10 Å radius from its center-of-mass (see Figure 7a in ref 15). The interaction between N_2 and the C_{168} channel intersection is significantly more attractive with the ab initio potential (open squares) than the Steele potential (open circles) for $r < 2.9$ Å due to the larger values of σ_{C-N} and ϵ_{C-N}, and is more repulsive for $r > 2.9$ Å. The interaction between O_2 and the C_{168} channel intersection is slightly more attractive with the ab initio potential (solid squares) than the Steele potential (solid circles) for $r < 2.9$ Å due to the larger value of σ_{C-O}, and is slightly more repulsive for $r > 2.9$ Å. Most importantly, there is a large difference between the interactions of N_2 and O_2 with the channel intersection calculated with the ab initio potential; however, the difference is rather small when the Steele potential is used. This is also the case for the extent of the adsorption of the two gases, as we shall see.

III. Method

Grand canonical Monte Carlo (GCMC) simulations[17,18] at fixed adsorbate chemical potential μ, volume V, and temperature

T were carried out for the adsorption of pure O_2 and N_2 and their mixture in the C_{168} schwarzite. Because the chemical potentials of adsorbate in the adsorbed and bulk phases are identical at thermodynamic equilibrium, GCMC simulation allows one to directly relate the chemical potentials of adsorbate in both phases, and has been used widely for the simulation of adsorption. The grand canonical ensemble is an open system in equilibrium with an infinite bulk fluid reservoir, and the number of absorbate molecules is allowed to fluctuate. During the simulation, random moves are performed by using a Markov process to generate a sequence of configurations.

In this work we consider gas adsorption at low and moderate pressures at temperature $T = 300$ K; as a consequence, we assume that the bulk gas and gas mixture are ideal gases. Nevertheless, at high pressures the nonideal effect should be taken into account, e.g., by an equation of state or by simulation at a fixed bulk pressure.[4,19] The simulation box representing the adsorbent consisted of 8 ($2 \times 2 \times 2$) C_{168} schwarzite unit cells with periodic boundary conditions in all three dimensions. A cutoff distance of 21.8 Å, half the simulation box length, was used in the evaluation of intermolecular interaction energies, and no long-range corrections were applied. A test using a larger simulation box of 27 ($3 \times 3 \times 3$) unit cells did not, within statistical error, give discernibly different results. The number of moves in a typical simulation was 2×10^7, though additional moves were used at high loadings. The first 10^7 moves were used for equilibration, and the second 10^7 moves to obtain ensemble averages.

For the adsorption of a pure gas, four types of trial moves were randomly attempted in the GCMC simulation, namely, displacement and rotation of a randomly chosen existing molecule, creation of a new molecule at a random position, and deletion of an existing molecule. To ensure microscopic reversibility, the creation and deletion were attempted with equal probability. For the adsorption from a mixture, in addition, exchange of molecule identity was used, i.e., O_2 to N_2 and vice versa, with equal probability. While this trial move is not required in the GCMC simulation, its use allows reaching equilibrium faster and reduces fluctuations after equilibration.[20]

The isosteric heat of adsorption, a way to characterize the adsorption process, is calculated by

$$q_{st} = RT - \left(\frac{dU}{dN}\right)_{T,V} \tag{1}$$

where R is the gas constant, U is the total adsorption energy, and N is the number of adsorbate molecules. To arrive at eq 1, it is assumed that the adsorption process is reversible, adsorption equilibrium is achieved, the bulk fluid is an ideal gas, and the internal degrees of freedom of the adsorbate molecule do not change appreciably upon adsorption.

In the limit of zero loading, the affinity between adsorbate and adsorbent is usually described by the Henry constant K_H and the zero-loading isosteric heat of adsorption q_{st}^0, both of which can be determined from the GCMC simulation. For example, K_H at temperature T can be obtained by extrapolating the adsorption isotherm to zero loading

$$K_H(T) = \lim_{P \to 0}(N/PV) \tag{2}$$

where P is bulk pressure and V is volume of absorbed phase. On the basis of the van't Hoff equation and assuming that q_{st}^0 is a constant over a temperature range between T_1 and T_2, q_{st}^0 can be obtained by

$$q_{st}^0 = R\left[\frac{\ln K_H(T_2) - \ln K_H(T_1)}{1/T_2 - 1/T_1}\right] \tag{3}$$

However, this approach to estimate the Henry constant and isosteric heat at zero loading requires a series of GCMC simulations. The better approach used in this work is to use canonical ensemble NVT Monte Carlo simulation with a single gas molecule to represent zero loading. In this case, q_{st}^0 can be calculated from[21]

$$q_{st}^0(T) = RT - \langle U_a \rangle \tag{4}$$

where $\langle U_a \rangle$ is the ensemble average of the interaction energy between an isolated gas molecule and an empty adsorbent. In this approach the temperature dependence of q_{st}^0 is obtained. K_H can be calculated by the Widom test-particle insertion method[22]

$$K_H(T) = \beta \exp(-\beta \mu_{ex}^0) \tag{5}$$

where $\beta = 1/(k_B T)$ and μ_{ex}^0 is the excess chemical potential of a single gas molecule in an empty adsorbent. In our recent study for the adsorption of N_2 on a variety of carbonaceous materials, we found that both approaches give results in close agreement.[23]

We also consider the use of the ideal-adsorbed-solution theory (IAST) developed by Myers and Prausnitz[24] to predict the adsorption of the O_2 and N_2 mixture based on the adsorption information obtained for the pure components. This theory is thermodynamically consistent and exact in the limit of zero pressure, and has served as a benchmark to calculate the adsorption of mixtures from the adsorption information for only the pure components. In this work, first, a two-site Langmuir model

$$N^\circ(P) = N_1^m \frac{k_1 P}{1 + k_1 P} + N_2^m \frac{k_2 P}{1 + k_2 P} \tag{6}$$

was used to fit the isotherms of pure O_2 and N_2, respectively, where N_i^m and k_i are adjustable parameters. For an O_2 and N_2 binary mixture, the equilibrium criterion from the IAST is

$$P_i = P_i^\circ(\pi_i) x_i \tag{7}$$

where P_i is the bulk pressure of gas i, x_i is the mole fraction of gas i in the adsorbed phase, and P_i° is the hypothetical pressure of pure gas i at the spreading pressure π_i when the bulk and adsorbed phases are in equilibrium. The Gibbs adsorption approach gives the spreading pressure π_i per unit area as

$$\pi_i = RT \int_0^{P_i^\circ} N_i^\circ(P)\, d\ln P \tag{8}$$

where N_i° is the adsorption isotherm of pure gas i fitted by eq 6. The mixing process is carried out at a constant spreading pressure, that is, for each component, we have

$$\pi_1 = \pi_2 = \pi \tag{9}$$

By solving eqs 7−9, the amount of each gas i adsorbed in the mixture can be calculated from

$$N_i = x_i \Big/ \left[\frac{x_1}{N_1^\circ(P_1^\circ)} + \frac{x_2}{N_2^\circ(P_2^\circ)}\right] \tag{10}$$

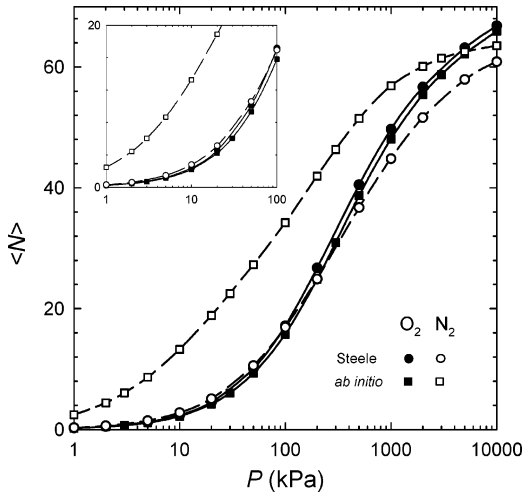

Figure 2. Adsorption isotherms of pure O_2 and N_2, respectively, reported as the number of admolecules per unit cell of the C_{168} schwarzite at 300 K. The solid (O_2) and open (N_2) circles are the Steele potential, the solid (O_2) and open (N_2) squares are the ab initio potential, and the lines are the fits of the two-site Langmuir model. The inset shows the low-pressure region.

TABLE 2: Parameters in the Two-Site Langmuir Model to Fit the Adsorption Isotherms of Pure O_2 and N_2, Respectively, at 300 K

		N_1^m	k_1 (1/kPa)	N_2^m	k_2 (1/kPa)
Steele	O_2	13.48	2.58×10^{-4}	58.44	4.04×10^{-3}
	N_2	31.67	1.05×10^{-3}	32.23	7.70×10^{-3}
ab initio	O_2	14.81	3.47×10^{-4}	55.76	3.80×10^{-3}
	N_2	23.28	1.00×10^{-1}	41.02	4.64×10^{-3}

Finally, the predictions from the IAST were compared with the GCMC simulation results.

IV. Results and Discussion

Figure 2 shows the adsorption isotherms from simulation for pure O_2 and pure N_2 reported as the number of admolecules per unit cell of the C_{168} schwarzite at 300 K as a function of bulk pressure. The inset shows the low-pressure region. Compared with the Steele potential, the ab initio potential consistently results in slightly less adsorption for O_2, but significantly larger adsorption for N_2. As previously reported,[3] with the Steele potential, the amounts of adsorption of the two pure gases are generally quite close; in contrast, with the ab initio potential, the amounts are substantially different. With both potentials, N_2 adsorbs more than O_2 at low pressures, and the reverse is found at high pressures. This is the consequence of several factors. First, the bond length l_{N-N} is shorter than l_{O-O}; and second, the collision diameter σ_{C-N} is larger than s_{C-O}. As we have verified in the previous study,[3] and in Figure S1 of the Supporting Information showing the variation of the adsorption isotherm of N_2 with the collision diameter σ_{C-N}, these factors lead to a stronger attraction for N_2 in the C_{168} schwarzite, and hence a greater adsorption of N_2 at low pressures. This is more evident with the ab initio potential as, in addition, the well depth ϵ_{C-N} is larger than ϵ_{C-O}. At high pressures, however, O_2 is preferentially adsorbed as O_2 has a smaller molecular size than N_2, and therefore can fit more easily into the partially filled pores. Finally, the lines in Figure 2 indicate the fits of the two-site Langmuir model to the simulation results of the pure gases, using the parameters given in Table 2. The fits are in excellent agreement with the simulation results at all pressures.

Table 3 gives the Henry constants and the isosteric heats for pure O_2 and N_2, respectively, at 300 K calculated from the NVT simulations in the limit of zero loading. The Henry constant of N_2 is 22% larger than that of O_2 with the Steele potential, and is 92% larger with the ab initio potential. The isosteric heat of N_2 is 4% larger than O_2 with the Steele potential, and 27% larger with the ab initio potential. For O_2 the values of both the Henry constant and the isosteric heat are close with both potentials; for N_2, however, the ab initio potential gives larger values of both quantities, again, indicating stronger adsorption than with the Steele potential.

TABLE 3: Henry Constant and Limiting Isosteric Heat of Pure O_2 and N_2 Adsorption, Respectively, at 300 K

	Steele potential		ab initio potential	
	O_2	N_2	O_2	N_2
K_H (mol/dm^3/kPa)	0.038	0.049	0.037	0.447
q_{st}^0 (kJ/mol)	21.12	21.98	21.17	28.85

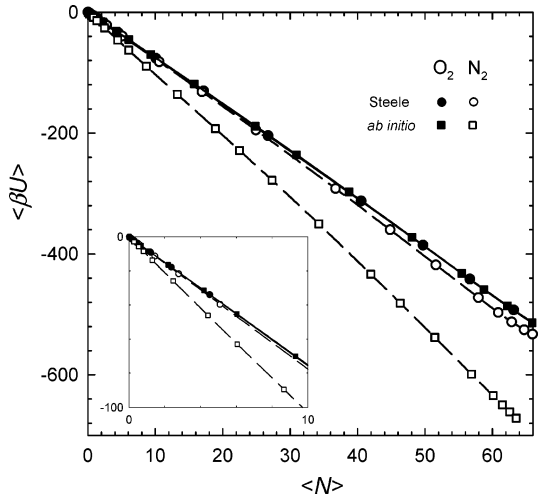

Figure 3. Adsorption energies of pure O_2 and N_2, respectively, at 300 K as a function of loading. The solid (O_2) and open (N_2) circles are the Steele potential, the solid (O_2) and open (N_2) squares are the ab initio potential, and the lines are to guide the eye. The inset shows the low-loading region.

Figure 3 shows the adsorption energies of pure O_2 and N_2, respectively, at 300 K as a function of loading, i.e., the number of admolecules per unit cell, and the inset shows the low-loading region. There are two contributions to the adsorption energy, one from the gas−gas interaction, and the other from the gas−adsorbent interaction. For O_2, the adsorption energies are nearly indistinguishable for the two potentials, and are consistently lower than N_2. For N_2, the adsorption energy calculated with the ab initio potential is much more attractive than that calculated with the Steele potential. Figure S2 of the Supporting Information shows the variation of the adsorption energy of N_2 with the collision diameter σ_{C-N}, and that a large value of σ_{C-N} results in an adsorption energy that is greater in absolute value.

Figure 4 shows the isosteric heats of pure O_2 and N_2, respectively, at 300 K as a function of loading. Extrapolated to zero loading, q_{st} here are approximately equal to q_{st}^0 values given in Table 3, which are calculated from the NVT simulations. For O_2, the values of q_{st} estimated with both potentials are close, as are their adsorption isotherms. With increasing O_2 loading, q_{st} increases slowly to a maximum and then decreases rapidly. Such behavior of the isosteric heat of adsorption has been observed experimentally, for example, the adsorption of Xe in zeolites X and Y,[25] of Ar in $AlPO_4$-5,[26] and of CH_4 in a fcc-structured silica gel.[27] For N_2, using the Steele potential, q_{st} is slightly larger than for O_2 but has a similar trend, i.e., increases slowly and then decreases rapidly with increasing

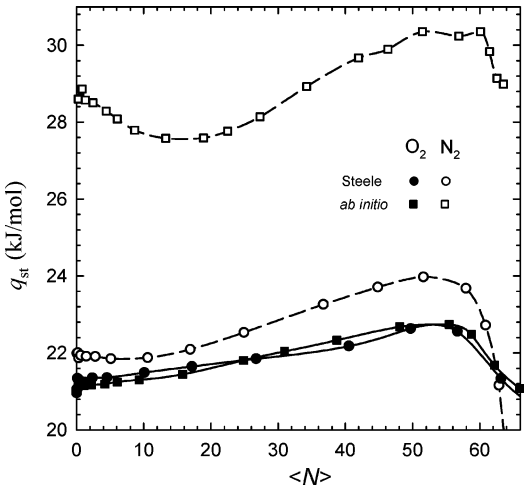

Figure 4. Isosteric heats of pure O_2 and N_2 adsorption, respectively, at 300 K as a function of loading. The solid (O_2) and open (N_2) circles are the Steele potential, the solid (O_2) and open (N_2) squares are the ab initio potential, and the lines are to guide the eye.

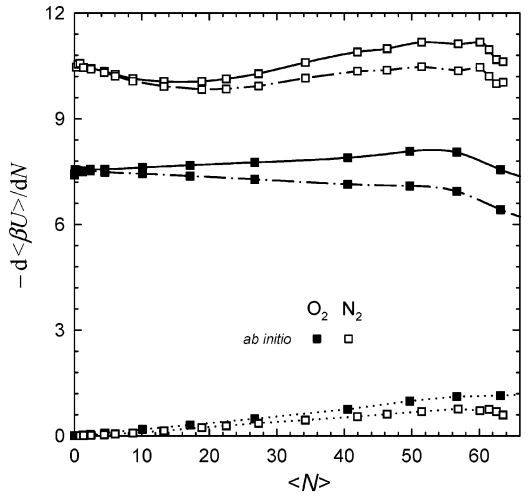

Figure 5. Derivatives of the adsorption energy with respect to loading for pure O_2 and N_2, respectively, at 300 K with the ab initio potential. The solid, dotted, and dot-dashed lines are the contributions from total, gas−gas, and gas−C_{168}, respectively.

loading. However, with the ab initio potential, q_{st} is much larger and shows different behavior. With increasing N_2 loading, q_{st} first decreases to a minimum, then increases to a maximum, and finally decreases. This type of behavior is not unusual and has been observed in previous experimental studies, such as the adsorption of N_2 and CO in $AlPO_4$-5,[26] of CH_4 in a silica gel with a hard sphere structure,[27] of Ar in chabazite,[28] and of CH_4 in activated carbon.[29]

To investigate the underlying physics of this observed behavior of the isosteric heat of adsorption, the derivative of the total adsorption energy with respect to the admolecule number in eq 1 is split into two terms, one for the gas−gas interaction, and the other for the gas−C_{168} interaction,

$$-\left[\frac{d(\beta U)}{dN}\right] = -\left[\frac{d(\beta U_{gas-gas})}{dN}\right] - \left[\frac{d(\beta U_{gas-C_{168}})}{dN}\right] \quad (11)$$

Figure 5 shows the values of these derivatives for O_2 and N_2, respectively, as a function of loading with only the ab initio potential. The solid, dotted, and dot-dashed lines are the total, gas−gas, and gas−C_{168} contributions, respectively. For both O_2 and N_2, the attraction between gas molecules increases upon adsorption in the C_{168} schwarzite, consequently, the derivative of gas−gas interaction increases. At high loadings, however, the derivative of gas−gas interaction decreases as the short intermolecular separation distance in the already filled pore space leads to a weak attraction. The derivative of the gas−C_{168} contribution is different for O_2 and N_2. For O_2, with increasing admolecule number it decreases slowly at low loadings, and rapidly at high loadings. Initially, the rate of increase in the O_2-O_2 contribution is larger than the rate of the decrease in the O_2-C_{168} contribution. Overall, the total derivative, and hence the isosteric heat, first increases slowly, and then decreases rapidly. For N_2, however, with increasing admolecule number the derivative of N_2-C_{168} first decreases to a minimum, then increases, and finally decreases again. The rate of change in the N_2-C_{168} contribution overwhelms that in the N_2-N_2 contribution, and as a consequence, the total derivative and the isosteric heat have the same trend as the N_2-C_{168} contribution. Figure S3 of the Supporting Information shows the variation of the isosteric heat of N_2 with the collision diameter σ_{C-N}. With a larger value of σ_{C-N}, as shown in Figures S1 and S2, respectively, there are enhanced adsorption and interaction energy, so that the isosteric heat is greater. In addition, the behavior of the isosteric heat changes with σ_{C-N} resulting in a minimum for σ_{C-N} approximately equal to 3.36 Å.

Figure 6 shows the density distribution of the centers-of-mass of adsorbed pure N_2 at 300 K and 1000 kPa generated by accumulating 50 equilibrium configurations. The linked network is the C_{168} schwarzite unit cell structure, and the points are the centers-of-mass of the N_2 molecules. The centers-of-mass are not distributed uniformly, but with a preference for alignment along the channel intersections, and localized in the small pores. With the ab initio potential, as the adsorption is greater, the localization in the small pores is more pronounced as seen in Figure 6b. In our previous study,[3] we have found that on going from low to high pressure (or equivalently chemical potential) with gradually increasing admolecules, the center-of-mass density distribution showed an interesting shift. At low pressures, the density distribution was nonuniform, but continuous in both types of pores. However, the distribution in the small pores became localized at modest pressures and, in particular, there were no admolecules at the center of the small pores. Finally, at high pressures, the center-of-mass distribution in the large pores also became localized.

The reason for this shift has been discussed[3] and is described briefly here. With increasing pressure, the gas−gas attraction first increases at low pressures, but then decreases at modest pressures. This is because as the number of admolecules increases there is an adsorbate−adsorbate repulsion in the small pores as a result of the limited available separation distance between the admolecules as more are adsorbed. In a competitive balance between energetic and entropic effects, a phenomenon similar to a phase separation occurs, leading to the localized density distribution in the small pores. However, the total interaction energy continues to increase as the number of admolecules increases, especially in the large pores. A further increase in pressure results in a further decrease in the adsorbate−adsorbate interaction energy. The same phenomenon that has occurred in the small pores then occurs in the large pores at high pressures.

Figure 7 shows the angular distribution as a function of $\cos\alpha$ for pure N_2 adsorption at 300 K and 1000 kPa, where α is the angle between the bond of a diatomic N_2 molecule and the z axis within the C_{168} schwarzite. The angular distribution deviates

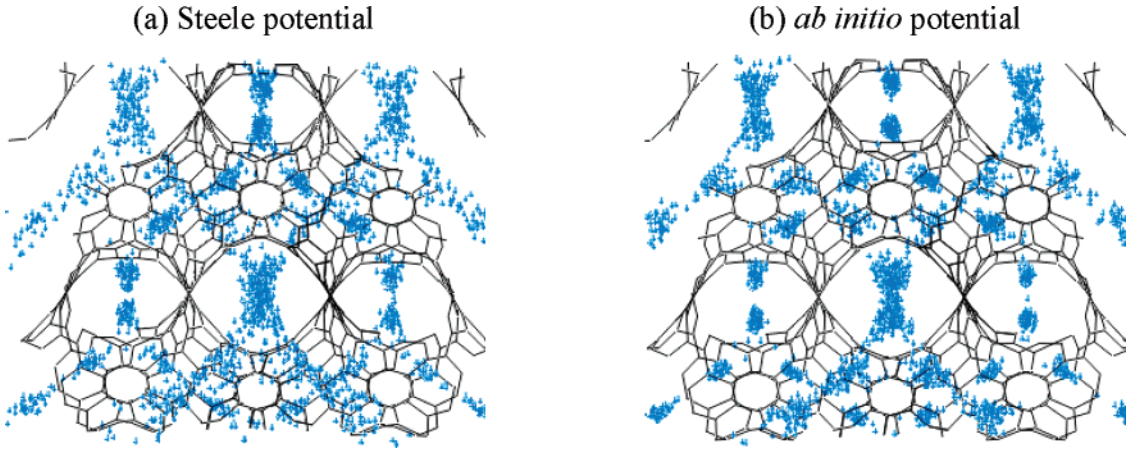

Figure 6. Center-of-mass density distribution of adsorbed pure N_2 molecules at 300 K and 1000 kPa generated by accumulating 50 equilibrium configurations: (a) Steele potential and (b) ab initio potential. Blue points are the centers-of-mass of N_2 molecules.

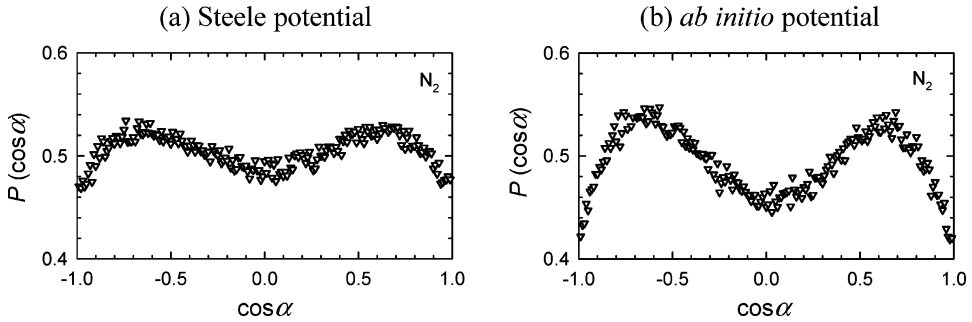

Figure 7. Angular distribution of adsorbed pure N_2 molecules at 300 K and 1000 kPa: (a) Steele potential and (b) ab initio potential.

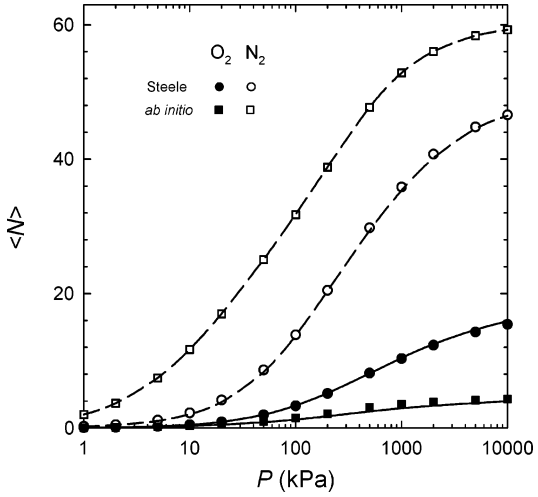

Figure 8. Adsorption isotherm of air at 300 K as a function of total bulk pressure. The solid (O_2) and open (N_2) circles are the Steele potential, the solid (O_2) and open (N_2) squares are the ab initio potential, and the lines are the IAST predictions.

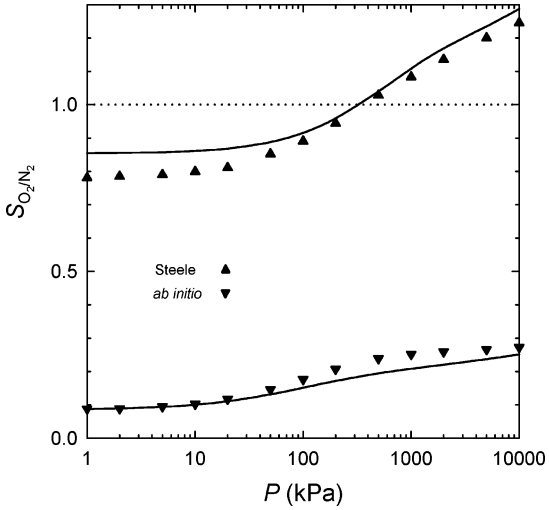

Figure 9. Selectivity of O_2 to N_2 from air adsorption as a function of total bulk pressure. The upper triangles are the Steele potential, the lower triangles are the ab initio potential, and the lines are the IAST predictions.

from 0.5 (a uniform angular distribution in the bulk), and has a maximum at $\alpha = 45°$ (and by symmetry at 135°). This indicates that the orientation of the N_2 molecule is somewhat preferentially aligned toward the channel intersections that connect pores in the neighboring layers at about 45° (and 135°) from the *z* axis. With the ab initio potential, as the adsorption is greater, the orientational preference is more evident in Figure 7b. We have previously observed[3] that this orientational preference tends to disappear with increasing pressure as the maximum in the angular distribution becomes less defined tending to a uniform distribution.

We next consider the adsorption of O_2 and N_2 from air (O_2:N_2 = 0.21:0.79). Figure 8 shows the adsorption isotherm as a function of total bulk pressure at 300 K. On the basis of the adsorption of pure O_2 and N_2, the predictions of the IAST are in excellent agreement with the GCMC simulation for both gases in the mixture with either potential. As the bulk partial pressure of N_2 is almost 4 times larger than O_2, and the adsorption of N_2 is energetically preferred at low pressures, N_2 adsorbs more than O_2 with both potentials over the whole range of pressure studied, and the amounts of both N_2 and O_2 increase with increasing pressure. Nevertheless, it can be expected that with increasing high pressures, although not shown, the size effect becomes dominant and the amount of O_2 will keep increasing and the amount of N_2 will decrease. At still higher

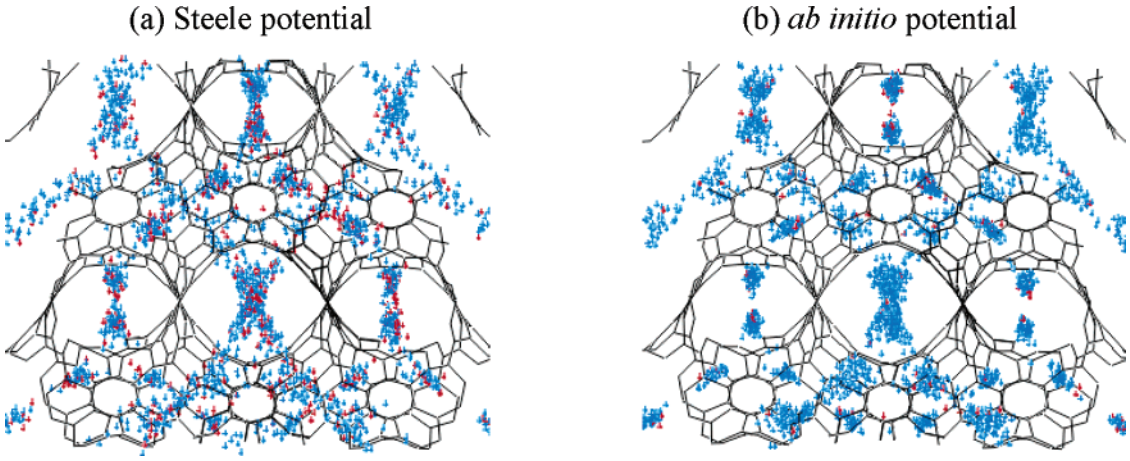

Figure 10. Center-of-mass density distributions of O_2 and N_2 molecules for air adsorption at 300 K and 1000 kPa generated by accumulating 50 equilibrium configurations: (a) Steele potential and (b) ab initio potential. Red points are the centers-of-mass of O_2 molecules, and blue points are the centers-of-mass of N_2 molecules.

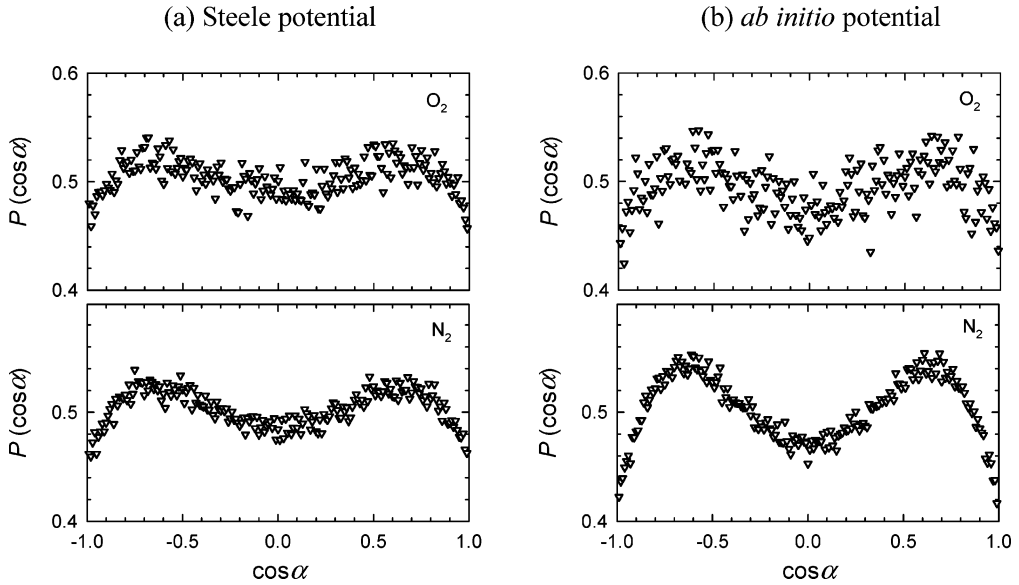

Figure 11. Angular distributions of O_2 and N_2 molecules for air adsorption at 300 K and 1000 kPa: (a) Steele potential and (b) ab initio potential.

pressures, the pores will be completely filled and the adsorption of both gases will reach saturation. Compared with the results using the Steele potential, the ab initio potential yields a larger difference between the amounts of adsorbed N_2 and O_2, that is, with the ab initio potential, the selectivity between the two gases from air is larger.

The selectivity of component i with respect to j is defined to be $S_{i/j} = (x_i/y_i)/(x_j/y_j)$, where x_i and y_i are the compositions of component i in the adsorbed and bulk phases, respectively. The selectivity is the key parameter to quantify the competitive adsorption between two components from their mixture. When $S_{i/j} > 1$ component i is preferentially adsorbed, and if $S_{i/j} < 1$ component j is preferentially adsorbed. Also, $S_{i/j} = 1$ implies that there is no preferential adsorption; it is the isoselective point (ISP) at which there is a selectivity reversal from $S_{i/j} < 1$ to $S_{i/j} > 1$ or vice versa.

Figure 9 shows the adsorption selectivity of O_2 to N_2, S_{O_2/N_2}, from air as a function of the bulk pressure. The upper and lower triangles are from the GCMC simulations with the Steele and ab initio potentials, respectively, and the solid lines are the predictions from the IAST. Reasonably good agreement between the simulations and the IAST predictions is obtained in both cases. With the Steele potential, S_{O_2/N_2} increases with increasing pressure in the range of this study, and the ISP is at about 500 kPa. For an equimolar O_2 and N_2 mixture, the ISP was also found to be at about 500 kPa,[4] indicating that in this case the ISP from the Steele potential does not change much with bulk composition, and the variation of bulk composition does not lead to selectivity reversal at a fixed pressure. This phenomenon has been observed in the experimental study of the adsorption of O_2-N_2 mixtures on anatase,[30] predicted from a theoretical analysis of the adsorption of hard rods on a linear substrate,[31] of square-well mixtures in one-dimension.[32] With use of the Steele potential, when the bulk pressure is lower than 500 kPa, S_{O_2/N_2} is less than 1 and N_2 is preferentially adsorbed, and when he bulk pressure is higher than 500 kPa, S_{O_2/N_2} is greater than 1 and O_2 is preferentially adsorbed. This is consistent with the above discussion that at low pressures N_2 adsorbs more strongly than O_2, but at high pressures O_2 can fit more easily into the partially filled pores. Overall S_{O_2/N_2} is close to 1, which shows that with the Steele potential no large separation between O_2 and N_2 is predicted. However, with the ab initio potential, there is slight increase in the selectivity with pressure, and over the whole pressure range of this study, no reversal occurs and S_{O_2/N_2} is consistently much less than 1, so that N_2 is more strongly adsorbed from the binary mixture, air, and the separation between the two gases is quite large. This suggests that the C_{168} schwarzite and other nanoporous carbon membranes might be

useful for air separation, for example, by pressure swing adsorption, if the mass transfer effects can be overcome.

Figure 10 shows the center-of-mass density distributions of O_2 and N_2 from air adsorbed in the C_{168} schwarzite at 300 K and 1000 kPa generated by accumulating 50 configurations. The black network is the C_{168} schwarzite unit cell structure, and red and blue points are the centers-of-mass of O_2 and N_2 molecules, respectively. As shown in Figure 8, compared with the Steele potential, the ab initio potential results in more adsorption for N_2 and less adsorption for O_2. Consequently, the center-of-mass distribution is denser for N_2 in Figure 10b with the ab initio potential, but is denser for O_2 in Figure 10a with the Steele potential. This can more clearly be seen in Figure S4 of the Supporting Information, in which the center-of-mass density distributions are shown separately for O_2 and N_2. Furthermore, the center-of-mass density distribution in Figure 10b is more localized in the small pores as more gas molecules are adsorbed, particularly N_2 molecules.

Figure 11 shows the angular distributions of O_2 and N_2 as a function of cosα for air adsorption at 300 K and 1000 kPa. Both depart from the value of 0.5 (a uniform angular distribution in the bulk), and show a maximum in α at 45° (and by symmetry at 135°), implying that there is an orientational preference of the admolecules in the direction of the channel intersections. For O_2, the maxima in parts a and b of Figure 11 with the Steele and ab initio potentials, respectively, are about the same. In Figure 11b, the angular distribution of O_2 is more scattered as fewer O_2 molecules are adsorbed as shown in Figure 8. However, for N_2, the maximum in Figure 11a with the Steele potential is smaller than that in Figure 11b with the ab initio potential, because N_2 has a stronger attraction with the C_{168} schwarzite calculated with the ab initio potential.

V. Conclusions

In this work we have investigated the adsorption of pure O_2 and N_2 and their mixture in the C_{168} schwarzite as an adsorbent model for a nanoporous carbon. Two types of potentials have been used for the additive atom−atom interaction of each gas with carbon schwarzite. One is the empirical Steele potential with parameters obtained by others from gas adsorption on planar graphite. The use of the Steele potential is based on the assumption that the hybridization of carbon atoms and the localization of electron densities are not affected by carbon surface curvature and carbon ring structure, thus are the same for both planar graphite and the C_{168} schwarzite. These important factors are taken into account in the ab initio potential with parameters obtained by us from first-principles quantum chemical computations for the gases interacting with the C_{168} schwarzite. This ab initio potential is expected to be more accurate. With the Steele potential, the predicted adsorption behavior does not provide an explanation of the high separation factors between O_2 and N_2 as both gases have similar adsorption properties. With the ab initio potential, however, we predict large adsorptive separation between the two gases in the C_{168} schwarzite, with N_2 adsorbing much more than O_2. That N_2 is adsorbed more strongly suggests, based on the arguments used to explain chromatographic separations, that O_2 will have a higher permeability through the C_{168} schwarzite. The results demonstrate that the accuracy of the interaction potential is crucial to accurately determining adsorption behavior, and that an inaccurate potential may result in large errors. Our results also suggest that the empirical Steele potential may not be applicable for carbon-based materials with a curvature and ring structure that are different from planar graphite. Finally, the results based on the ab initio potential suggest that nanoporous carbon adsorbents, such as the C_{168} schwarzite, can be useful for air separation.

Acknowledgment. We acknowledge the financial support under Contracts CTS-0083709 and EEC-0085461 from the National Science Foundation, and Contract DE-FG02-85ER13436 from the Department of Energy.

Supporting Information Available: Variations of the adsorption isotherm, adsorption energy, and isosteric heat of N_2 with the collision diameter σ_{C-N}; center-of-mass density distributions of O_2 and N_2, separately, for air adsorption. This material is available free of charge via the Internet at http://pubs.acs.org.

References and Notes

(1) Shiflett, M. B.; Foley, H. C. *Science* **1999**, *285*, 1902.

(2) Shiflett, M. B.; Pedrick, J. F.; McLean, S. R.; Subramoney, S.; Foley, H. C. *Adv. Mater.* **2000**, *12*, 21.

(3) Jiang, J. W.; Klauda, J. B.; Sandler, S. I. *Langmuir* **2003**, *19*, 3512.

(4) Jiang, J. W.; Sandler, S. I. *Langmuir* **2003**, *19*, 5936.

(5) Bojan, M. J.; Steele, W. A. *Langmuir* **1987**, *3*, 116.

(6) Bojan, M. J.; Steele, W. A. *Langmuir* **1987**, *3*, 1123.

(7) Madhav, A.; Foley, H. C. *AIChE J.* **2000**, *46*, 911.

(8) Rallabandi, P. S.; Ford, D. M. *AIChE J.* **2000**, *46*, 99.

(9) Nicholson, D. Intermolecular Forces and Simulation in Pores. In *Physical Adsorption*: *Experiment*, *Theory and Applications*; Fraissard, J., Ed.; Kluwer Academic Publishers: Dordrecht, The Netherlands, 1997; p 105.

(10) Sandler, S. I.; Sum, A. K.; Lin, S.-T. Some Chemical Engineering Applications of Quantum Chemical Calculations. In *Advances in Chemical Engineering*; Chakraborty, A., Ed.; Academic Press: San Diego, CA, 2001; Vol. 28, p 313.

(11) Vanderbilt, D.; Tersoff, J. *Phys. Rev. Lett.* **1992**, *68*, 511.

(12) Laufer, J. C.; Leroi, G. E. *J. Chem. Phys.* **1971**, *55*, 993.

(13) Murthy, C. S.; Sing, K.; Klein, M. L.; McDonald, I. R. *Mol. Phys.* **1980**, *41*, 1387.

(14) Klauda, J. B.; Garrison, S. L.; Jiang, J. W.; Arora, G.; Sandler, S. I. *J. Phys. Chem. A* **2004**, *108*, 107.

(15) Klauda, J. B.; Jiang, J. W.; Sandler, S. I. *J. Phys. Chem. B*, **2004**, *108*, 9842.

(16) Frisch, M. J.; Trucks, G. W.; Schlegel, H. B.; Scuseria, G. E.; Robb, M. A.; Cheeseman, J. R.; Zakrzewski, V. G.; Montgomery, J. A.; Stratmann, R. E.; Burant, J. C.; Dapprich, S.; Millam, J. M.; Daniels, A. D.; Kudin, K. N.; Strain, M. C.; Farkas, O.; Tomasi, J.; Barone, V.; Cossi, M.; Cammi, R.; Mennucci, B.; Pomelli, C.; Adamo, C.; Clifford, S.; Ochterski, J.; Petersson, G. A.; Ayala, P. Y.; Cui, Q.; Morokuma, K.; Malick, D. K.; Rabuck, A. D.; Raghavachari, K.; Foresman, J. B.; Cioslowski, J.; Ortiz, J. V.; Stefanov, B. B.; Liu, G.; Liashenko, A.; Piskorz, P.; Komaromi, I.; Gomperts, R.; Martin, R. L.; Fox, D. J.; Keith, T.; Al-Laham, M. A.; Peng, C. Y.; Nanayakkara, A.; Gonzalez, C.; Challacombe, M.; Gill, P. M. W.; Johnson, B. G.; Chen, W.; Wong, M. W.; Andres, J. L.; Head-Gordon, M.; Replogle, E. S.; Pople, J. A. *Gaussian 98*, Revision A.11.3; Gaussian, Inc.: Pittsburgh, PA, 2002.

(17) Allen, M. P.; Tildesley, D. J. *Computer simulation of liquids*; Clarendon Press: Oxford, UK, 1987.

(18) Frenkel, D.; Smit, B. *Understanding Molecular Simulations*: *From algorithms to applications*, 2nd ed.; Academic Press: San Diego, CA, 2002.

(19) Jiang, J. W.; Sandler, S. I. *Phys. Rev. B* **2003**, *68*, 245412.

(20) Kofke, D. *Mol. Simul.* **1991**, *7*, 285.

(21) Nicholson, D.; Parasonage, N. G. *Computer simulation and the statistical mechanics of adsorption*; Academic Press: New York, 1982.

(22) Widom, B. *J. Chem. Phys.* **1963**, *39*, 2802.

(23) Jiang, J. W.; Wagner, N. J.; Sandler, S. I. Unpublished.

(24) Myers, A. L.; Prausnitz, J. M. *AIChE J.* **1965**, *11*, 121.

(25) Woods, G. B.; Rowlinson, J. S. *J. Chem. Soc., Faraday Trans. 2* **1989**, *85*, 765.

(26) Grillet, Y.; Llewellyn, P. L.; Tosi-Pellenq, N.; Rouquerol, J. *Adsorption of Argon, Methane, Nitrogen, Carbon Monoxide and Water Vapour on Sepiolite and AlPO4-5 as Studied by Isothermal Microcalorimetry*; Fundamentals of adsorption: proceedings of the Fourth International Conference on Fundamentals of Adsorption, 1992, Kyoto, Japan.

(27) Vuong, T.; Monson, P. A. *Langmuir* **1996**, *12*, 5425.
(28) Rudzinski, W. Fundamentals of Single-Gas and Mixed-Gas Adsorption on Heterogeneous Solid Surfaces. In *Physical Adsorption*: *Experiment, Theory and Applications*; Fraissard, J., Ed.; Kluwer Academic Publishers: Dordrecht, The Netherlands, 1997; p 181.
(29) Choi, B. K.; Choi, D. K.; lee, Y. W.; Lee, B. K.; Kim, S. H. *J. Chem. Eng. Data* **2003**, *48*, 603.
(30) Arnold, J. R. *J. Am. Chem. Soc.* **1949**, *71*, 104.
(31) Talbot, J. *AIChE J.* **1997**, *43*, 2471.
(32) Heuchel, M. *Langmuir* **1997**, *13*, 1150.